Proceedings of ICMEM2007
International Conference on Mechanical Engineering and Mechanics
November 5-7, 2007, Wuxi, China

Stability Analysis and Simulation of the Vibration Behavior of Worm Gears in Drive Systems

Hans DRESIG
Institut für Mechanik, TU Chemnitz, 09107 Chemnitz, Germany
e-mail: hans.dresig@mb.tu-chemnitz.de

Uwe SCHREIBER, Paul RODIONOW
ITI Gesellschaft für ingenieurtechnische Informationsverarbeitung mbH, 01219 Dresden, Germany
e-mail: schreiber@iti.de, rodionow@iti.de

Abstract: Self-locking worm gears have the advantage, that they can position loads, blocking any further movements. This feature exploits the physical effect of self-locking. This provides an efficient solution, since any further locking devices, such as brakes, can be omitted. A load of arbitrary dimension is safely held in position even if the motor is turned off.
In practical applications the exploitation of self-locking is not free of problems. Under certain circumstances chatter vibrations can arise, which have a negative impact on comfort and noise generation, increase wear, and can lead to instabilities, which render impossible the operation of the equipment.
The paper examines the influence of various parameters on the occurrence of chatter phenomena – analytically for systems with few degrees of freedom as well as numerically for complex vibratory systems. The results are summarized in stability charts as functions of similarity indicators and are discussed. Known charts are extended by the additional condition of damping influence.
The developed physical vibratory model for the worm gear considers its relevant geometry, mass, and stiffness parameters. The model permits the simulation of arbitrary worm gears under considering the interactions with the surrounding vibratory components of drive, output side, and bearings. Complex drive systems with manifold nonlinearities are hardly accessible via analytic solutions. Using simulation, additional driveline factors influencing the dynamic behavior (and the chatter in particular) are identified, which exceed the conclusions from analytical solutions found in hitherto existing directives.
The paper provides the design engineer with utilities and tools for preventing chatter vibrations in worm gears. Examples from practice demonstrate the effectiveness of various measures which can be taken in order to avoid chatter. Physical and mathematic interrelationships are explained and tools are provided with which the design engineer can forecast or avoid chatter vibration in drive trains with worm gears. Practical examples demonstrate the effect of different methods.

Keywords: Vibrations, Parametric Excitation, Self-Locking, Chatter, Stability Chart, Physical Modeling, System Simulation and Optimization

1 Introduction

It is state of the art in the estimation of dynamic loads in machine drive systems, that specialized models are developed for typical components. Consequently, there are specialized software tools for spur gears, planetary gears [7], crank mechanisms, belt drives, and many other machine parts [8].

This paper introduces a computational model for worm gears. This nonlinear model has the peculiarity, that it cannot be linearized any more, even for vibrations with comparatively small amplitudes. Due to backlash and friction, the model structure (i.e., the number of degrees of freedom) change in dependence of the state of vibration. As a consequence, the classical stability concept cannot be applied to worm gears. Over time the worm gear passes regions, where vibration amplitudes grow exponentially (classical instability), which then are followed by regions, where the vibrations are damped (stable). In the sequel we consider all cases as "unstable", where the vibrations grow over a certain period of time, because this already leads to destructively large amplitudes.

In the development of drives containing worm gears it is important to know, how the system parameters influence the appearance of chatter vibrations. Thereby the boundaries of instability regions are of particular interest. These dangerous areas must be avoided during operation. The VDI Guideline 2158 [6] states: „Chatter is the continuing change of the contact surfaces of the force-transmitting elements in gearboxes." The guideline assesses the stability of a driveline against chatter using just a few parameters of the corresponding rigid-body system, cf. also [1].

Often chatter is considered to be caused by the difference between the static and kinetic friction coefficients or a decreasing friction characteristic. In reality, also stiffnesses, dampings, and backlashes have an influence on chatter vibrations. These effects are considered in the publications of Oledzki [2], Veiz [3], and Jiang/Steinhilper [4], [5], which also give stability charts. The damping influence was rendered more precisely in [9]. The questions about the influence of additional parameters or neighboring vibratory components are still unresolved. This study is going to show, that chatter vibrations can also arise for constant friction coefficients and how the resulting dynamic loads can be computed. Of particular interest is the influence of tooth geometries, rotational speeds, backlashes, inertias, external loads, stiffnesses and dampings in the drive and the gears, as well as frictions, on the self-excited vibrations and the resulting vibration loads in the complete drive system.

2 Theoretical Background, Explained on the Simple Example of a Worm Gear with Elastic Drive Shaft

2.1 Equations of Motion

First, the model depicted in Figure 1 und Figure 2 is examined. It is composed of the following components, which have 12 parameters:

Torsional stiffness and damping of the drive shaft	k_T, d_T
Radius of the worm wheel and inertia on the worm shaft	r_1, J_1
Stiffness and damping of the toothing	k_V, d_V
Pressure angle of the teeth, pitch angle of the worm	α_n, γ
Backlash and friction coefficient in the tooth contact	δ, μ
adius of the gear wheel and inertia on shaft 2	r_2, J_2

In addition to the parameters, the angle $\varphi_0(t)$, the torque $M_1(t)$ on the worm, and the output torque $M_2(t)$ can be given. By setting the appropriate $\varphi_0(t)$, the startup, stationary operation, and braking of the model in Figure 1 and Figure 2 can be described. So, in contrary to [5], there is no assumption of the drive to run at constant speed only. Braking torques on the worm resulting from bearing friction can be assigned to M_1. The model permits to find parameter sets for stable (i.e., chatter-free) as well as unstable (with chatter) operation in an analytical way. This procedure is explained in the sequel.

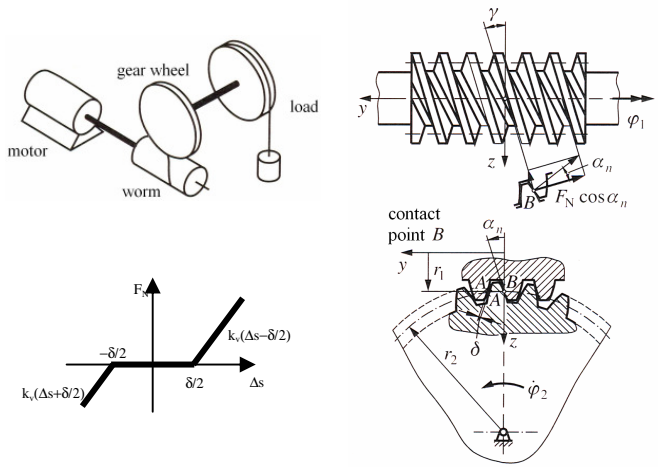

Figure 1: Hoisting unit with worm gear

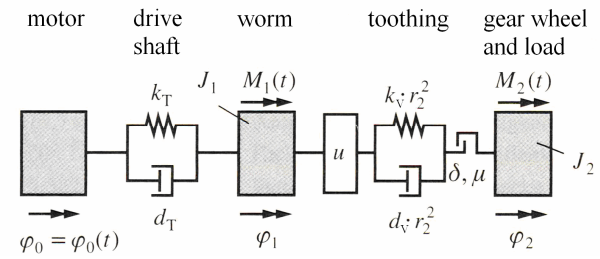

Figure 2: Model of a worm gear with elastic drive shaft and toothing with elasticity and backlash

The equations of motion for the model depicted in Figure 2 follow, e.g., from the dynamic torque balance equations of the rotary masses (cf. [8] and [9]):

$$J_1\ddot{\varphi}_1 + (d_T + d_V c_1)\dot{\varphi}_1 + (k_T + k_V c_1)\varphi_1 - d_V c_1 u\dot{\varphi}_2 - k_V c_1 u\varphi_2 = \ldots = M_1 + sign(\Delta\varphi)k_V c_2\frac{\delta}{2} + k_T\varphi_0 + d_T\dot{\varphi} \quad (1)$$

$$J_2\ddot{\varphi}_2 - d_V c_3\dot{\varphi}_1 - k_V c_3\varphi_1 + d_V c_3 u\dot{\varphi}_2 + k_V c_3 u\varphi_2 = \ldots = M_2 - sign(\Delta\varphi)k_V c_4\frac{\delta}{2} \quad (2)$$

The transmission ratio u of a worm gear without backlash is defined as

$$u = r_2/(r_1\cdot\tan\gamma), \quad (3)$$

The transmission ratio relates the angle φ_1 on the drive side to the angle φ_2 on the driven side as $\varphi_1 = u\varphi_2$. Due to elasticity and backlash in the toothing there appears a relative angle

$$\Delta\varphi = \varphi_1 - u\varphi_2, \quad (4)$$

which corresponds to a relative displacement

$$\Delta s = r_1\cos\alpha_n\sin\gamma\,\Delta\varphi \quad (5)$$

at the tooth contact point in normal direction (cf. Figure 1). If the worm and the gear wheel are in contact, a response torque is assumed, which depends linearily from the relative displacement and the relative speed. The teeth are deformed, if $|\Delta s| > \delta/2$.

The angles $\varphi_1(t)$ and $\varphi_2(t)$ can be computed by a numerical integration of equations (1) and (2). After solving the differential equations, all other quantities of interest can be computed, such as rotary speeds and accelerations, the torque M_{an} in the drive shaft (cf. (6)) and the tangential force F_V in the reference circle of the tooth contact according to (7).

$$M_{an} = k_T\cdot(\varphi_1 - \varphi_0) + d_T\cdot(\dot{\varphi}_1 - \dot{\varphi}_0) \quad (6)$$

$$F_V = \left[k_V c_3(\varphi_1 - u\cdot\varphi_2) + d_V c_3(\dot{\varphi}_1 - u\dot{\varphi}_2) + sign(\Delta\varphi)k_V c_4\frac{\delta}{2}\right]/r_2 \quad (7)$$

The coefficients c_k in (1) and (2) depend on the sign of the relative angle $\Delta\varphi$ and on the speed $\dot{\varphi}_1$. This can be expressed by defining a parameter S as:

$$S = sign(\Delta\varphi)\cdot sign(\dot{\varphi}_1) = sign(\Delta\varphi\cdot\dot{\varphi}_1) \quad (8)$$

For the response torques the coefficients according (9) to (12) are obtained, following the derivations given in [4] and [5]. The coefficients describe the tangential components of the dynamic friction force.

$$c_1 = r_1^2\cdot c_1^* = r_1^2\cdot\cos^2\alpha_n\cdot\sin\gamma\cdot\sin[\gamma + \rho\cdot S)]/\cos\rho \quad (9)$$

$$c_2 = r_1\cdot c_2^* = r_1\cdot\cos\alpha_n\cdot\sin[\gamma + \rho\cdot S]/\cos\rho \quad (10)$$

$$c_3 = r_1\cdot r_2\cdot c_3^* = r_1\cdot r_2\cdot\cos^2\alpha_n\cdot\sin\gamma\cdot\cos[\gamma + \rho\cdot S]/\cos\rho \quad (11)$$

$$c_4 = r_2\cdot c_4^* = r_2\cdot\cos\alpha_n\cdot\cos[\gamma + \rho\cdot S]/\cos\rho \quad (12)$$

Within the backlash, i.e. for $|\Delta s| < \delta/2$, the contact forces and thus the coefficients c_k equal zero. The friction angle ρ results from the friction coefficient μ and the pressure angle α_n of the toothing:

$$\rho = \arctan(\mu/\cos\alpha_n) \quad (13)$$

2.2 Derivation of the Conditions for Stability

Chatter vibrations do not arise inherently, but only if the parameters of the drive system are located in a region of instability. The boundaries of such regions can be estimated using classical approaches, i.e. without solving the differential equations.

The estimation of stability boundaries starts with the consideration, that the first two coefficients c_1 and c_2 can become negative for self-locking worm gears (i.e., for $\gamma < \rho$). This can only happen, if $S = -1$, which means that the signs of the rotary speed $\dot{\varphi}_1$ and the relative angle $\Delta\varphi$ are different from each other. This happens if the load is lowered ($\dot{\varphi}_1 > 0$) and a preload ($\Delta\varphi < 0$) exists in the direction of motion or if the load torque M_2 acts in the direction of motion.

The coefficients c_3 and c_4 are positive in all operating modes, since $\cos[\gamma + \rho \cdot S]$ does not become negative due to the small values of γ and ρ.

In order to assess the stability, an exponential ansatz and the linearization of (1) and (2), which is applicable for small oscillation amplitudes, are used (Lyapunov). From the characteristic equation

$$\begin{vmatrix} J_1\lambda^2 + (d_T + d_V c_1)\lambda + (k_T + k_V c_1) & -d_V c_1 u\lambda - k_V c_1 u \\ -d_V c_3\lambda - k_V c_3 & J_2\lambda^2 + d_V c_3 u\lambda + k_V c_3 u \end{vmatrix} = 0 \quad (14)$$

or, respectively, the 4th-order characteristic polynomial

$$P(\lambda) = \lambda^4 + b_1 \cdot \lambda^3 + b_2 \cdot \lambda^2 + b_3 \cdot \lambda + b_4 = 0 \quad (15)$$

with the coefficients

$$\begin{aligned} b_1 &= (d_T + c_1 d_V)/J_1 + u c_3 d_V / J_2 \\ b_2 &= (k_T + c_1 k_V)/J_1 + u c_3 k_V / J_2 + u c_3 d_T d_V /(J_1 J_2) \\ b_3 &= u c_3 (d_T k_V + d_V k_T)/(J_1 J_2) \\ b_4 &= u c_3 k_T k_V /(J_1 J_2) \end{aligned} \quad (16)$$

the four eigenvalues $\lambda_i = \delta_i + j\,\omega_i$ can be computed. The real parts δ_i of these eigenvalues define the damping, whereas the imaginary parts ω_i define the natural frequency (angular frequency). The motion of the worm gear is stable, if and only if the real parts of all four eigenvalues are negative.

The coefficients b_1 and b_2 can become negative, if c_1 is negative. b_3 and b_4 are always positive, since c_3 is always positive. In an undamped system $b_1 = 0$ and $b_3 = 0$ is hold. Using the ROUTH-HURWITZ criterion it can be estimated without solving (15), whether at least one of the four eigenvalues has a positive real part. After some short derivations, this leads to the following three conditions for negative real parts δ_i of the eigenvalues or for a stable motion respectively:

$$b_1 > 0 \quad (17)$$

$$b_1 b_2 - b_3 > 0 \quad (18)$$

$$b_1 b_2 b_3 - b_1^2 b_4 - b_3^2 = (b_1 b_2 - b_3) b_3 - b_1^2 b_4 > 0 \quad (19)$$

Condition (18) holds, if condition (19) holds, which is due to the positive signs of b3 and b4. This implies, that a stable motion of a worm gear with elastic drive, as depicted in Figure 2, is possible, if the conditions (17) and (19) are fulfilled. The motion becomes unstable, if one of the conditions does not hold. From condition (17) follows the first condition for instability:

$$\frac{J_1}{J_2} < \frac{-c_1}{u \cdot c_3} - \frac{d_T}{d_V \cdot u \cdot c_3} = \frac{\tan(\rho - \gamma)}{u^2 \cdot \tan(\gamma)} - \frac{d_T \cdot \tan(\gamma)}{d_V \cdot r_2^2 \cdot c_3^*} \quad (20)$$

Chatter vibrations arise in the worm gear, if the inequality (20) becomes true. This can happen only for $c_1 < 0$ or $S = -1$ respectively, and thus only for self-locking worm gears. For $d_T = 0$ the inequality becomes identical to condition (21) derived by FÜSGEN (cf. [1]), which became part of the VDI Guideline 2158 (equation (49) therein).

$$\frac{J_1}{J_2} < \frac{\tan(\rho - \gamma)}{u^2 \cdot \tan(\gamma)} \quad (21)$$

It is well known, that from the first condition for instability (20) follows, that the risk of chatter vibrations grows for increasing friction angles ρ, decreasing pitch angles $\gamma$and decreasing transmission ratios u. An increase of the torsional damping d_T in the drive shaft reduces the interval of instability for a given ratio J_1 / J_2. According to the condition (20) an increase in the damping d_V of the toothing or of the coefficient $c_3^* / \tan(\gamma)$ reduces the stabilizing effect of the torsional damping d_T.

It is interesting to note, that the toothing stiffness k_V and the torsional stiffness k_T do not influence condition (20). The backlash δ, the load torque M_2, and the motion $\varphi_0(t)$ do also not affect the stability boundaries, but they determine the intensity of the self-excited vibrations in the unstable region.

(19) forms the **second condition for instability**. This condition also describes the influence of the elastic drive. However, the condition is so complicated, that it is impossible to derive straightforward relationships in an analytical way. Instead, the condition must be evaluated numerically for the parameter ranges of interest.

In the sequel, the damping constants d_T and d_V , which bear physical units of measurement, are substituted by the dimensionless damping measures D_T and D_V respectively. These follow from the relationships (22) and (23). For large transmission ratios u they correspond to the dimensionless LEHR's damping values.

$$d_T = 2 \cdot D_T \cdot \sqrt{k_T \cdot J_1}\ [N \cdot m \cdot s] \quad (22)$$

$$d_V \cdot r_2^2 = 2 \cdot D_V \cdot \sqrt{k_V \cdot r_2^2 \cdot J_2}\ [N \cdot m \cdot s] \quad (23)$$

In addition, a dimensionless damping ratio is introduced using: $D_{TV} = D_T / D_V$

$$\frac{d_T}{d_V \cdot r_2^2} = \frac{D_T}{D_V} \cdot \sqrt{\frac{k_T \cdot J_1}{k_V \cdot r_2^2 \cdot J_2}} = D_{TV} \cdot \sqrt{\frac{k_T \cdot J_1}{k_V \cdot r_2^2 \cdot J_2}} \quad (24)$$

The product $(D_{TV} \cdot r_2)$ has the same meaning as the damping coefficient α in [5] and can be used for result comparisons.

2.3 Generation and Interpretation of Stability Charts

The following fixed parameter set for the worm gear, as found in [4], [5], and [8], is used:

$$\alpha_n = 20°,\ \gamma = 5.3228°,\ \mu = 0.132\ (\rho = 8°), \quad (25)$$

$$r_1 = 3.235\,mm,\ r_2 = 18.98\,mm\ (u = 63),\ J_2 = 0.1\ kg \cdot m^2$$

$$k_V = 1.7728 \cdot 10^6\ N/m,\ d_V = 1250\,N \cdot s/m \quad (26)$$

$$(D_V = 0.028)$$

In the computations the inertia J_1 ranges from $10^{-6}\ kg \cdot m^2$ to $10^{-3}\ kg \cdot m^2$, the torsional stiffness k_T from $5 \cdot 10^{-3}\ N \cdot m$ to $5\,N \cdot m$.

Figure 3 shows the boundaries between the stable (above the lines) and the unstable (below the lines) region according to the first condition for instability (20), if the torsional damping is dT = 0. The chart illustrates the

parameter influences, which are described by the classical FÜSGEN criterion (21).

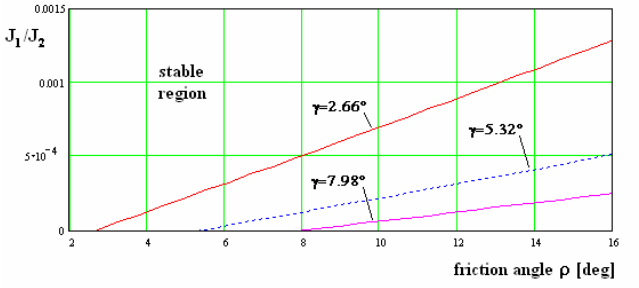

Figure 3: Stability boundaries according to the first criterion (20), depending on friction angles ρ and pitch angles γ (the stable region is situated above the lines)

An increase of the torsional damping d_T reduces the unstable interval for the ratio J_1/J_2 compared to the chart in Figure 3. The increase of the damping d_V in the tooth contact or of the coefficient $c_3^*/\tan(\gamma)$ reduces the stabilizing effect of d_T according to condition (20). Also, (20) defines an unstable region for small friction coefficients and very small ratios J_1/J_2. The boundaries of the region depend on the stiffnesses of the drive shaft and the tooth contact.

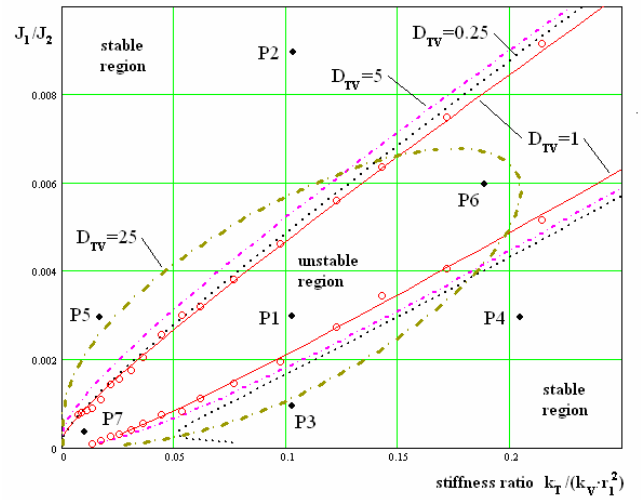

Figure 4: Stability chart for $D_V = 0.014$ according to the second criterion (19)

Figure 4 shows the stability boundaries according to the **second condition for instability** (19) for $S = -1$, a torsional damping d_T and a tooth contact damping d_V following from (22) and (23), and $D_V = 0.014$. Additional computations for the same parameter set have confirmed, that there are no unstable regions for $S = +1$.

As can be seen from Figure 4, the unstable region for a damping ratio $D_{TV} = 25$ has an oval shape. There is no instability for stiffness ratios $k_T/(k_V \cdot r_1^2)$ bigger than 0.22. For the damping ratio $D_{TV} = 5$ the unstable region has an oval shape too. However, it appears more narrow and stretched. For stiffness ratios larger than 1 there is also no unstable region (outside the displayed area in Figure 4).

It is interesting to note, that for small stiffness ratios the unstable region for J_1/J_2 broadens with increasing damping ratio D_{TV} (compare, e.g., the unstable regions for $D_{TV} = 5$ and $D_{TV} = 25$ and small stiffness ratios <0.10).

The unstable region for the damping ratio $D_{TV} = 1$ according to the second criterion has also an oval shape. For stiffness ratios bigger than 3 there is no instability (outside of the displayed area in Figure 4). The boundaries of the unstable region for $D_{TV} = 1$ coincide well with experimental results from [5], which are marked by little circles in Figure 4. Also, $D_{TV} = 1$ results in the smallest instability region. The region broadens for smaller as well as bigger for D_{TV}.

It follows from Figure 4, that the unstable region becomes shorter and broader with an increasing damping measure D_T. Apparently, the increase in torsional damping does not influence some of the design variants.

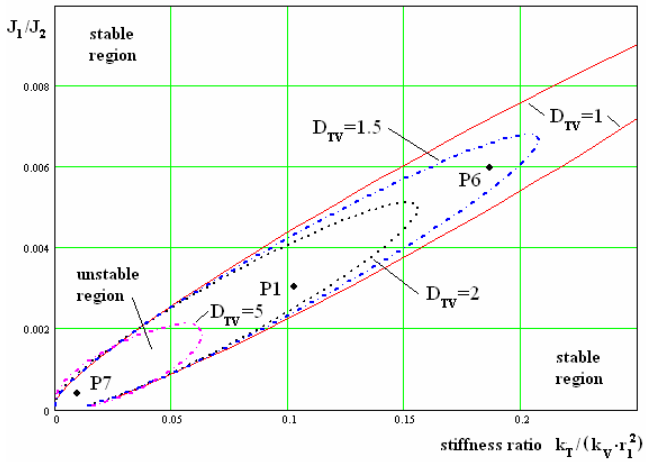

Figure 5: Stability boundaries for $D_V = 0.056$ according to the second criterion

Figure 5 shows, that for a damping measure $D_V = 0.056$ ($d_V = 2500$ Ns/m) all unstable regions are smaller than for the damping measure $D_V = 0.014$ ($d_V = 625$ Ns/m) as seen in Figure 4. The unstable region for $D_{TV} = 25$ virtually ceased to exist in Figure 5. The unstable region for the damping ratio $D_{TV} = 5$ became shorter by about 15 times. It has an oval shape and covers a very small area.

If follows from Figure 5, that the increase of the damping measure D_V of the tooth contact together with a constant damping ratio D_{TV} reduces the area of the unstable region. However, in some design variants the increase of the tooth contact damping D_V has no influence.

Using stability charts the designer can estimate, which parameter changes help to leave the dangerous unstable region. Depending on the location of the operating point in the unstable region an increase or a decrease of the ratios of inertias or stiffnesses may be feasible (this is already known from [4] and [5]). The boundary curves are closed from the right. So, under consideration of the damping, there can be found further stable operating points, where the ratios of inertias as well as damping are increased. These points can be used in order to stabilize the system without modifying the natural frequencies. Another option for a reduction of the unstable region and

the achievement of stable operating conditions is the increase of the damping measures D_T and D_V.

3 Example: Paper Reel Changer

3.1 Analytical Solution for a Paper Reel Changer

A paper reel changer is part of a printing machine, which supplies a new paper reel to the machine once the old one has finished. For one full rotation, using a lever, the heavy reel is first lifted by 90 degrees, than – continuing the rotation - is lowered and finally is lifted by 90 degrees again.

Figure 6 shows a sketch of a paper reel changer with a worm gear drive. The paper reel with a mass $m_2 = 175\,kg$ is mounted to a frame, which is connected to the worm gear via a drive shaft. The load torque results from the weight of the paper reel and depends on the current angle of the frame and the lever arm $l_2 = 1{,}2\ m$:

$$M_2 = m_2 \cdot g \cdot \cos\varphi_2 \cdot l_2 \qquad (27)$$

During one rotation of the frame the load torque acts in the direction of the rotation during the lowering of the load, as well as against the direction of rotation when the load is lifted.

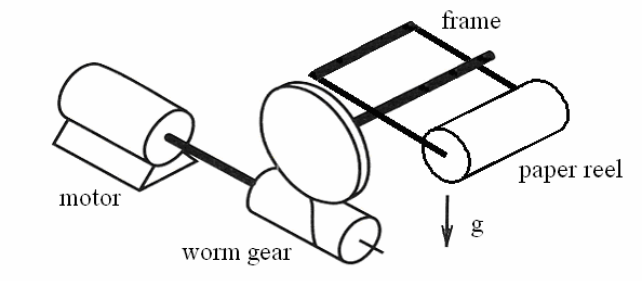

Figure 6: Paper reel changer with worm drive

The original parameters of the worm drive are given as follows (cf. Figure 1 and Figure 2):

$$\alpha_n = 20°,\ \gamma = 5.3228°,\ \mu = 0.134\ \ (\rho = 8°),$$
$$r_1 = 18.05\,mm,\ r_2 = 105.95\,mm\ (u = 63),$$
$$J_2 = 33\ kg \cdot m^2,\ k_V = 2 \cdot 10^8\ N/m,\ d_V = 21470\,N \cdot s/m$$
$$(D_V = 0.014) \qquad (28)$$
$$J_1 = 0.1\ kg \cdot m^2,\quad k_T = 7000\,N \cdot m,\ d_T = 0.74\overline{1}\,N \cdot m \cdot s$$
$$(D_T = 0.014)$$

For the given parameters the coefficients b_1, b_2, b_3, b_4 according to (16) are computed as $b_1 = 13.615\ s^{-1}$, $b_2 = 1.279 \cdot 10^5\ s^{-2}$, $b_3 = 9.004 \cdot 10^5\ s^{-3}$, $b_4 = 4.224 \cdot 10^9\ s^{-4}$. For these values condition (19) evaluates as $b_1 b_2 b_3 - b_1^2 b_4 - b_3^2 = -2.607 \cdot 10^{10}\,s^{-6} < 0$, which implies that the worm drive is unstable. Condition (21), $b_1 = 13.615 s^{-1} > 0$, implies a stable drive. This shows that the consideration of condition (21) only is insufficient for the stability assessment.

In the stable case $S = +1$ the eigenvalues are $\lambda_{1,2} = (-2.3 \pm 209.0 \cdot i)s^{-1}$ and $\lambda_{3,4} = (-5.8 \pm 328.1 \cdot i)s^{-1}$ with the corresponding damped natural frequencies f_1 = 33.3 Hz and f_2 = 52.2 Hz ($f_i = \omega_i/(2\pi)$). The corresponding LEHR damping values are $D_1 = \delta_1/\omega_1 = 0{,}011$ and $D_2 = \delta_2/\omega_2 = 0.017$. For $S = -1$ the eigenvalues are $\lambda_{1,2} = (-30.4 \pm 261.3 \cdot i)s^{-1}$ and $\lambda_{3,4} = (23.1 \pm 262.9 \cdot i)s^{-1}$ with the corresponding damped frequencies f_1 = 41.9 Hz und f_2 = 42.0 Hz. The positive real part of the eigenvalues 3 and 4 indicates that the oscillations with frequencies at about 42 Hz are unstable.

For the given parameters (28) the worm gear corresponds to the point **P1** in Figure 4 (with $k_T/(k_V \cdot r_1^2) = 0.107$ on the x axis and $J_1/J_2 = 0.003$ on the y axis). Apparently, **P1** belongs to the unstable region. Figure 4 also indicates that stability can be achieved either through an increase or through a decrease of the inertia J_1 as well as of the torsional stiffness.

3.2 Dynamic Analysis of the Vibration Behavior

3.2.1 General Remarks

Using numerical simulation, drives incorporating worm gears can be comprehensively analyzed. For any drive configuration, no matter how it is structured and how many components are part of the system, the simulation can assess, whether chatter vibration will occur or not. The shape of the self-excited vibrations (and thus the dynamic loads on the components) can be observed, even in the case of chatter.

The worm gear can be analyzed as part of a more complex drive system too, where, e.g., motor and brake characteristics or drive motions are defined by prescribed characteristics. This allows examining the combination of forced and self-excited vibrations even in the nonlinear case. Such solutions cannot be found in an analytical way.

It will be shown in the sequel, that the conclusions drawn from the stability charts can be confirmed by numerical simulation. Under closer examination the simulation results can deepen significantly the understanding of the physical processes. The results presented in this paper were achieved using the commercial simulation tool SimulationX [10].

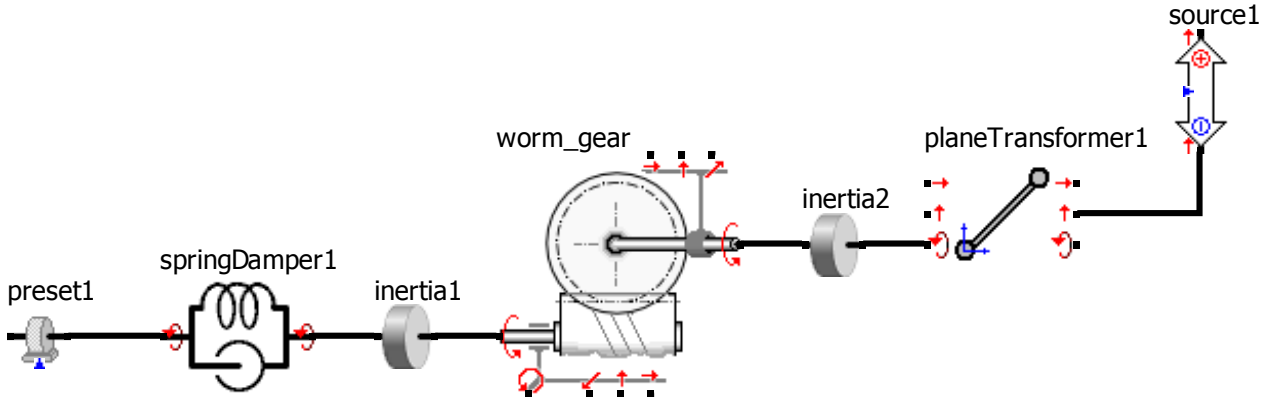

Figure 7: Model of the paper reel changer with elastic drive shaft im SimulationX

3.2.2 *Time-Domain Simulation for the Unstable Parameter Set P1*

The examination of the influence of backlash, drive speed, or load torque on the complete system requires the numerical integration of the equations (1) and (2). It is also necessary for the computation of force and motion quantities and their amplitudes over time. Using a simulation tool the user does not have to worry about the numerical integration himself.

Figure 7 shows the simulation model for a paper reel changer with elastic drive shaft. This model corresponds to the model in Figure 2, with φ_0 being the rotation angle of the motor, φ_1 the rotation angle of the worm, and φ_2 the rotation angle of the gear wheel and the frame. The drive parameters as given in (28) correspond to the point **P1** in Figure 4, so that chatter vibrations are to be expected.

The load torque is computed from the weight (source1) multiplied by the lever arm (planeTransformer1) and depends on the angular position of the reel changer (cf. (27)). The maximum load torque is M_2=2060 Nm. First, the backlash is assumed to be zero δ=0.

At the start of the simulation the frame is aligned horizontally. The first movement is upwards, i.e. the reel is lifted. The motor speed is n_0 = 472.5 rpm, the average speed of the worm is n_2 = 7.5 rpm. Consequently, the rotary speed of the frame is $\dot{\varphi}_{2m} = \Omega_R = 2\pi/8$ rad/s, i.e., one full rotation is completed in 8s. Figure 8 depicts the simulation results for this model. The chatter vibrations start, once the reel has passed the topmost position at t = 2 s. The chatter continues for the complete lowering phase, which lasts 4 s.

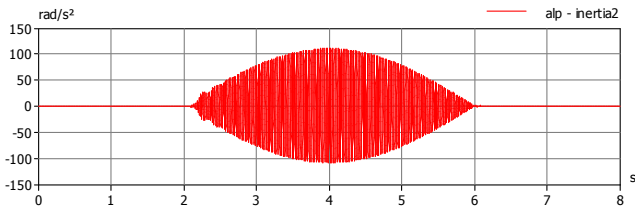

Figure 8: Angular acceleration $\ddot{\varphi}_2$ over time for the elastic drive without backlash (one full rotation in 8 s)

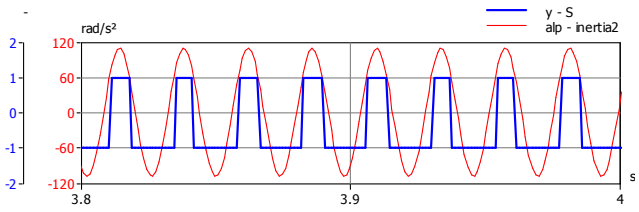

Figure 9: Angular acceleration $\ddot{\varphi}_2$ (zoomed section of the graph in Figure 8) and parameter S for the backlash-free reel changer with elastic drive

Figure 9 shows a zoomed section of Figure 8, together with the parameter S according to (8). The shape of the chatter vibration seems to be sinusoidal on the first glance, but it is composed of two sections. Due to the permanent change between stable ($S = +1$) and unstable ($S = -1$) behavior a stationary scenario with finite amplitudes in the chatter vibration builds up. Since the sign of the speed $\dot{\varphi}_1$ is constant, the parameter S depends only on the relative angle $\Delta\varphi$ (i.e., only on the contact flank).

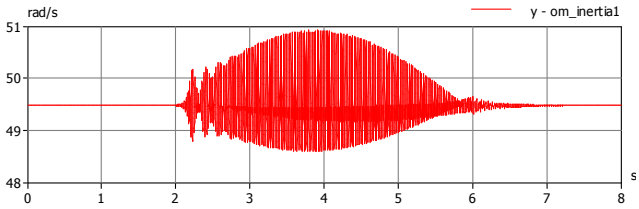

Figure 10: Rotary speed $\dot{\varphi}_1$ over time for the reel changer with elastic drive (for one full rotation in 8 s)

In self-locking worm gears ($\gamma < \rho$) arise chatter vibrations, if the quantity S according to (8) equals -1 and if at least one of the two conditions for instability becomes true. During one period the sign of S might be change. In this case, an interval with growing oscillation amplitudes is followed by an interval with decaying amplitudes. Thus, the „unstable“ chatter vibrations contain phases of rising as well as shrinking oscillation amplitudes within one vibration period. This is clearly observable from the time functions.

The angular acceleration amplitude of the gear wheel during chatter in the load lowering phase is virtually proportional to the load torque and has its maximum at $\ddot{\varphi}_2$ =110 rad/s^2. The main frequency of the chatter is about 42 Hz (see the eigenvalue computation above) and is located between the two natural frequencies of the stable system (33 Hz and 52 Hz). In this variant, there is no interaction between the natural vibrations and the chatter vibrations. If the chatter frequency gets closer to the natural frequencies, interactions take place and the maximum amplitudes of the chatter vibrations grow.

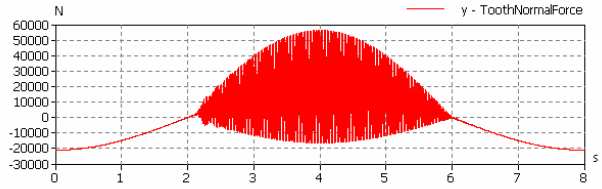

Figure 11: Normal forces in the tooth contact (left and right flank) for the reel changer with elastic drive and without backlash (for one full rotation in 8 s)

Figure 11 shows that the tooth contact forces during chatter (middle of the graph) can exceed the static mean value many times.

Parametric variations unveiled that the angular acceleration amplitudes do not depend on the rotary speed. However, when doubling the load torque the maximum acceleration amplitude is also doubled.

The impact of a backlash between the tooth flanks in the worm gear is illustrated in Figure 12. The backlash affects the system in particular for small load torques (i.e., for a small preload). After the backlash has been passed due to the direction change of the load torque, for 2-3 seconds after starting the load lowering there are contacts on both tooth flanks. This is observed in particular for larger backlash. The amplitudes become 2-4 times bigger than for the backlash-free case (cf. Figure 11).

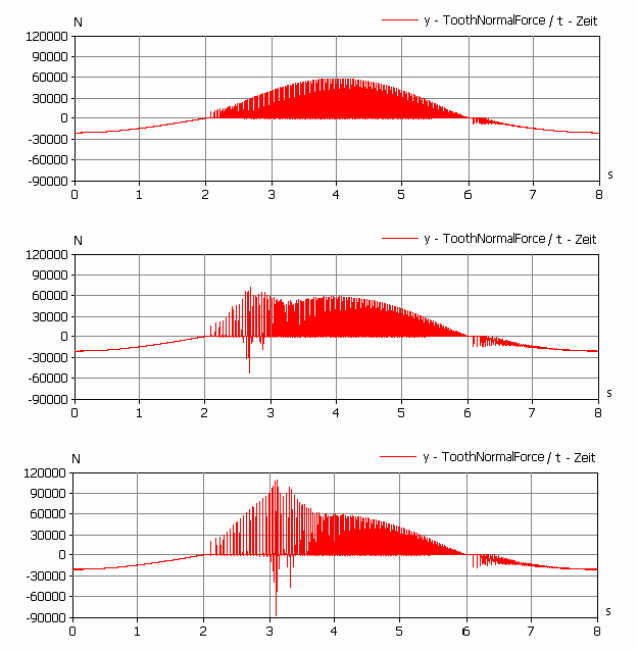

Figure 12: Normal force at teeth over time for the reel changer with elastic drive (point P1) and backlashes of δ = 0.25, 0.5, and 0.75mm (top to bottom; one full rotation in 8 s)

3.2.3 Time-Domain Simulation for the Unstable Parameter Set P7

Figure 13 to Figure 17 show the time functions for the reel changer without backlash using the parameter set P7 in Figure 4 (i.e., with a ten times smaller inertia J_1 and a ten times smaller stiffness k_T compared to the original parameter set P1 (28)).

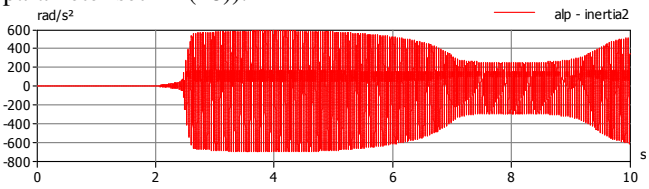

Figure 13: Angular acceleration of the gear wheel $\ddot{\varphi}_2$ during the lifting of the load for the parameter set P7 (there is also chatter during lifting)

First: The maximum acceleration during load lowering (interval from 2 s to 6 s in Figure 13) reaches about 700 rad/s^2. It is 5.5 times bigger than for the parameter set **P1** in Figure 8.

Reason: The natural frequencies of the system (81 Hz and 21 Hz) are close to twice the chatter frequency and half the chatter frequency. When lowering the load the worm shaft initially oscillates with the chatter frequency 41.8 Hz (cf. Figure 15). These vibrations excite the natural oscillations at 81 and 21 Hz. Within the time interval from 2.3 s to 2.6 s the excitation with the resonance-like responses can be seen. The amplitudes of the forced vibrations reach their maximum values very quickly. Afterwards the system oscillates "stationary" with frequencies around 31 Hz=(21+41)/2 Hz and 61 Hz=(81+41)/2 Hz (see Figure 14).

Second: In Figure 14 the contact parameter S changes its sign several times within one period.

Reason: As seen in Figure 15, the originally positive speed of the worm (upper red line *om_inertia1*) reaches zero and even small negative values due to the oscillations. Consequently, the parameter S changes sign several times per period, depending on the flank contact (positive or negative relative angle $\Delta\varphi$) and the rotary speed $\dot{\varphi}_1$.

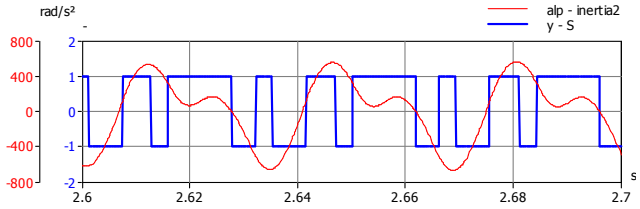

Figure 14: Angular acceleration $\ddot{\varphi}_2$ of the gear wheel (zoomed section of Figure 13) and parameter S during load lowering for the parameter set P7

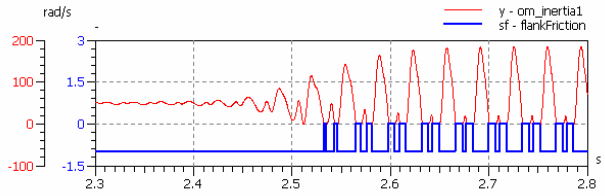

Figure 15: Rotary speed $\dot{\varphi}_1$ of the worm and parameter *sf* of the flank friction for the parameter set P7 during load lowering

Third: The blue (lower) curve *sf-flankFriction* in Figure 15 shows the state *sf* of the friction between the tooth flanks in the worm gear (0 – sticking, +1 or -1 - sliding). Apparently, the friction contact sticks for small rotary speeds $\dot{\varphi}_1$ of the worm. The sticking friction (together with the self-locking) brakes the oscillations and restricts the amplitude growth.

Fourth: In this variant the chatter vibrations continue into the lifting phase in the interval between 6 s and 10 s and do not die out (cf. Figure 13)**.**

Reason: Figure 16 shows a segment of Figure 13 during lifting in a time interval from 7.9 s to 8 s (end of the full rotation) and the corresponding parameter S. There are several segments per period, where S becomes negative. As a consequence the system becomes unstable also in the lifting phase. The time intervals, where $S=-1$, cover about 40 % of a period. The energy brought into the system in these phases is large enough to continue to excite the chatter. Thus, chatter is possible during the lifting phase too. If in the stable phases the vibrations are not damped strongly enough (due to low damping or strong excitation in the unstable phases), the chatter will persist. Then a small excitation will be sufficient for exciting and keeping alive the chatter.

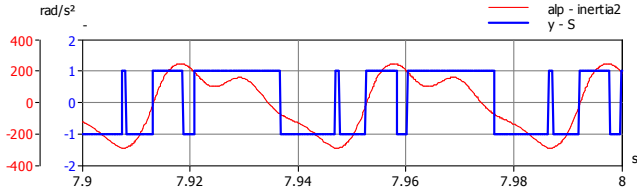

Figure 16: Angular acceleration $\ddot{\varphi}_2$ of the gear wheel (zoomed section of Figure 13) and parameter S during lifting for the parameter set P7

There are different **influences** of parameter variations for this reel changer with parameter set **P7**. The doubling of the drive speed of the motor is virtually double the vibration amplitudes.

Figure 17 illustrates the influence of the backlash in the tooth contact for the parameter set **P7.** The maximum amplitude of the normal force (about 280 kN) is virtually independent of the backlash in the interval from 0 to 0.75 mm. The bigger the backlash, the earlier the vibration dies out in the lifting phase. So, the backlash stabilizes the system.

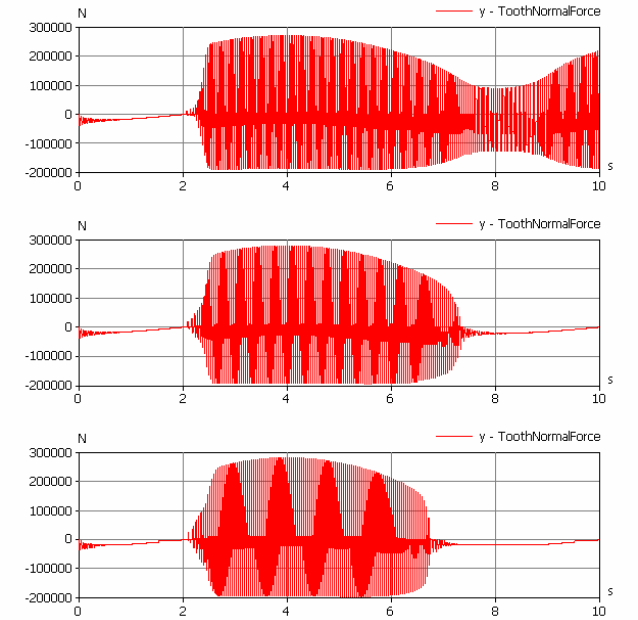

Figure 17: Normal force at teeth for the reel changer with elastic drive (parameter set P7) for backlashes δ =0.25, 0.5 and 0.75mm (from top to bottom) during one full rotation in 8 s.

3.2.4 *Time-Domain Simulation for Stable Parameter Sets*

If the inertia J_1 is tripled to 0.3 kgm², the simulation shows no chatter during the load lowering, albeit S is negative all the time. This coincides with the location of the parameter point **P2**, which is situated in the stable region in Figure 4. Figure 18 shows the respective drive shaft torque and the evolution of the parameter S. S equals -1 during lowering. When lifting the load, the torque is about 5 times bigger than in the lowering phase (due to the self-braking of the worm gear).

Comparable simulation results are obtained for the inertia J_1=0.033 kgm², which is three times smaller than in (28) (cf. **P3** in the lower stable region in Figure 4). Also, the variation of the shaft stiffness k_T (two times bigger or five times smaller than in the base parameter set (28)) gives the same results as shown in Figure 18. All lowering phases are stable. These parameter variants are reflected by the points **P4** and **P5** in Figure 4, which belong to the stable region.

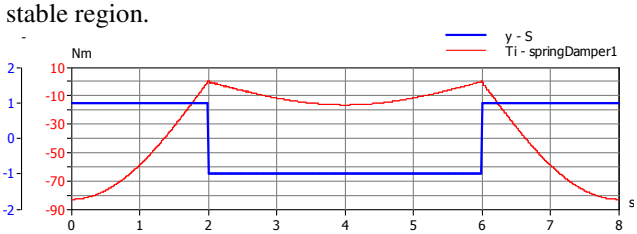

Figure 18: Drive shaft torque and parameter S in a reel changer with elastic drive and without backlash for the stable parameter set P2

Another parameter variation is described by the point **P6**: $J_1 = 0.2$ kgm², $k_T = 12000$ Nm/rad, $D_{TV} = 2$. This point belongs to the unstable region in Figure 4 (for the damping measure $D_V = 0.014$). For an increased damping measure $D_V = 0.056$ the point moves to the stable region (cf. Figure 5). Consequently, the simulation for $D_V = 0.056$ does not show chatter vibrations and gives the same results as seen in Figure 18.

3.2.5 *Consideration of Neighboring Components*

In practical applications the worm gear, which is the core of the model described here, is enclosed by further vibratory components. An estimation of the influence of additional masses and dampers on the drive side as well as on the driven side with respect to the FÜSGEN condition (21) is found in [6], an estimation with respect to condition (19) in [9].

For real systems these statements can only provide a rough orientation, since the additional drive components contribute several new masses and stiffnesses, which dynamically interact. In this case, reliable results are only achievable via simulation.

Here this shall be illustrated using an unstable worm gear which is parameterized such, that it corresponds to point **P1** in Figure 4.

Compared to Figure 7 the additional inertia *inertia4* (see Figure 19) on the drive side increases the equivalent drive mass and thus the inertia ratio J_1 / J_2. This implies that the point **P1** moves towards **P2** in the upper stable region. If the additional inertia and the stiffness of *springDamper1* are large enough and the stiffness of *springDamper4* is small enough, the worm gear becomes stable. Otherwise the system remains unstable and further interaction between the chatter vibrations and natural vibrations are possible.

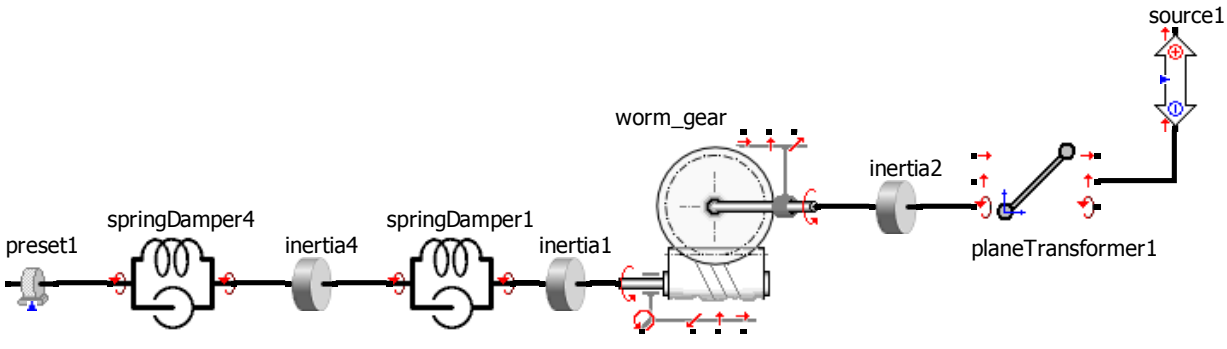

Figure 19: Model of the worm gear with additional inertia and elasticity on the drive side

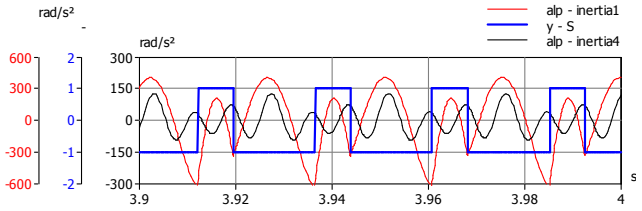

Figure 20: Accelerations $\ddot{\varphi}_1$, $\ddot{\varphi}_4$ of the inertias *inertia1* and *inertia4* and parameter S (bold line) in the model according to Figure 19

In the model as seen in Figure 19 the *inertia4* introduces a third natural frequency of 116 Hz. This frequency is close to the third multiple of the chatter frequency (42 Hz*3=126 Hz). As a consequence the chatter vibrations very strongly excite vibrations in the natural frequency of 122 Hz, which is located between the natural frequency of 116 Hz and the third harmonic of the chatter at 126 Hz. This is well visible in the acceleration of *inertia4* in Figure 20.

Summary

The presented vibratory model for the worm gear covers the essential geometry, mass, stiffness, and damping parameters as well as friction.

It was shown, under which conditions self-excited chatter vibrations arise in worm gears with a flexible drive shaft and an elastic gear contact – even for a constant friction coefficient.

For vibratory systems with 2 degrees of freedom stability charts can be computed, from which parameter regions for stable as well as unstable operations can be derived.

Due to the permanent change between stable (damped) and unstable (excited) ranges there arise periodic oscillations with finite amplitudes. A numerical simulation provides quantitative predictions about vibration amplitudes and component loads - also for the chatter vibrations.

The stability of the system depends on the damping ratio D_{TV} as well as on the absolute value of the damping measures (D_T and D_V). The unstable regions shrink with increasing D_V of the toothing and for a constant damping ratio D_{TV}.

The backlash does not influence the location of the stable regions, but it influences the dynamic loads. There are parameter ranges, where the dynamic load decreases with increasing backlash.

The presented worm gear model can be coupled to other drive components in a modular way as it is done, e.g., in the program SimulationX.

SimulationX can simulate arbitrary worm gears, their interactions with neighboring vibratory components on the drive side or on the driven side, as well as the influence of the bearings.

It is recommended to use these tools for the dimensioning of worm gears in drive systems in order to construct safe and economic products.

References

[1] Füsgen, P.: Untersuchungen über das Auftreten des Ratterns bei selbsthemmenden Schneckengetrieben und seine Verhütung. Forschungsberichte des Wirtschafts- und Verkehrsministeriums Nordrhein-Westfalen, 1954, Nr. 66. (in German)

[2] Oledzki, A.: Dynamics of Permanent Self-locking Systems. Int. Mechanisms, Vol.4, pp.105 – 138, Pergamon Press 1969.

[3] Veiz, V.L.: Dinamika mashinnykh aggregatov Leningrad: Mashinostroenie, 1969. (in Russian)

[4] Jiang, F.: Ratterschwingungen bei selbsthemmenden Schneckengetrieben. PhD thesis, Universität Kaiserslautern, 1989. (in German)

[5] Jiang, F.; Steinhilper, W.: Das Schwingungsverhalten von selbsthemmenden Schneckengetrieben und Maßnahmen zur Vermeidung von Ratterschwingungen. VDI Berichte Nr. 905, S.165-184, Düsseldorf: VDI-Verlag, 1991. (in German)

[6] VDI-Richtlinie-2158: Selbsthemmende und selbstbremsende Getriebe. Berlin: Beuth Verlag GmbH 1991. (in German)

[7] Dresig, H.; Schreiber, U.: Vibration Analysis for Planetary Gears, Modeling and Multibody Simulation. Proceedings of ICMEM2005, Vol.1, p 24 – 28. October 2005, Nanjing, China.

[8] Dresig, H.: Schwingungen mechanischer Antriebssysteme. Berlin: Springer-Verlag, 2. Auflage, 2006. (in German)

[9] Dresig, H.; Schreiber, U.; Rodionow, P.: Schwingungsberechnung und Stabilitätsanalyse von Schneckengetrieben im Antriebsstrang. VDI Berichte Nr. 1968, S. 71-94, Düsseldorf: VDI-Verlag, 2006. (in German)

[10] User Manual SimulationX 2.0, ITI GmbH Dresden, 2006.

[11] Dresig, H.; Holzweißig, F.: Maschinendynamik. Berlin: Springer-Verlag, 8. Auflage, 2007. (in German)